Combustion and Flame 248 (2023) 112585

Contents lists available at ScienceDirect

Combustion and Flame

journal homepage: www.elsevier.com/locate/combustflame

Regime and morphology of polyhedral bunsen flames

Yue Weng, Aditya Potnis, Abhishek Saha*

Department of Mechanical and Aerospace Engineering, University of California San Diego, La Jolla, CA 92093, USA

ARTICLE INFO

Article history:
Received 12 July 2022
Revised 10 December 2022
Accepted 11 December 2022
Available online 28 December 2022

ABSTRACT

Intrinsic flamefront cellular instabilities wrinkle, otherwise smooth, laminar flamefronts leading to excess surface area and, thus, burning rate. Since such instabilities increase flame propagation speed and burning rate without any external influence, such as turbulence, they are of both fundamental and practical interest. While extensively studied for freely propagating expanding or planar flames, cellular instabilities can also occur in burner-stabilized premixed flames. In this study, we present an experimental investigation of flamefront polyhedral instability occurring in premixed Bunsen flames for practically relevant lean hydrogen mixtures. Through systematic experiments, we delineate the effect of flame temperature, Lewis number, and flow rate on the stability and morphology of such flames. The results are presented as regime maps to clearly identify the conditions for which the flame manifests the instabilities and further illustrate how the transitional boundaries shift due to changes in experimental conditions. Moreover, the morphology of the flames was also investigated by identifying changes in the polyhedral structure as a function of operating conditions. Finally, we explain the observed dynamics of the polyhedral flames with the aid of analyzes of dispersion relation and residence time.

1. Introduction

With the growing concern about the environmental impacts of traditional combustion processes, in recent years, close attention has been paid to reducing carbon emissions from energy-producing devices. Besides initiating programs on the development of renewable energies, strict regulations and restrictions are being placed on the combustion of fossil fuels. Although the usage of renewable energy, including wind and solar, has gained momentum in the last few years, it is generally believed that combustion will still occupy the largest share of the energy supply for the next few decades. Thus, the development of new strategies for producing cleaner energy from combustion becomes critical in meeting the world's energy demand with limited negative impacts on the environment. With its capability to produce zero carbon emission, hydrogen has gained global attention as a future energy-friendly fuel [1–4]. In particular, lean premixed hydrogen combustors are becoming increasingly popular for gas turbines and other industrial applications [5]. However, using hydrogen poses certain challenges for its usage as a sustainable energy source, including its lower explosion limits and, thus, difficulty in storage. Moreover, because hydrogen is significantly lighter than the air, hydrogen/air mixtures are susceptible to combustion instabilities, including flamefront instability. Once the flamefront instability is triggered, cellular patterns appear on the flamefront and modify the smooth morphology of the premixed laminar flame. This wrinkling of the smooth flamefront, even in the absence of any external influences, increases the flame surface area and significantly alters the burning rate.

Flamefront cellular instabilities can be of two modes [6,7]. The Darrieus-Landau (hydrodynamic) instability occurs due to a sharp temperature gradient across the flamefront and is particularly critical at high-pressure conditions [8,9]. The diffusional-thermal cellular instability, on the other hand, occurs as a result of weaker thermal diffusion than mass diffusion, as noted by the sub-unity Lewis number, $Le < 1$ [10–12]. Here, Le is defined as the ratio between thermal to mass diffusivities of the mixture. Modern combustors operate at high-pressure, and crucially, combustion occurs at off-stoichiometric conditions (and hence non-unity Le), both of which increase the likelihood of cellular instabilities. Further, in these systems, these instabilities compete with turbulence to become the dominating mechanism that controls the dynamics of flame propagation [13–16]. Thus, cellular instabilities are practically relevant from the perspective of the performance and operation of these devices. To that end, a large volume of theoretical, modeling, and experimental research has been devoted to various aspects of cel-

* Corresponding author.
E-mail address: asaha@eng.ucsd.edu (A. Saha).

https://doi.org/10.1016/j.combustflame.2022.112585

lular instabilities, particularly in the context of idealized planar flames and unbounded propagating expanding flames. These studies have identified critical parameters to describe the onset of instabilities [17–19], their growth [20–25], stages of propagation [26], degree of acceleration [23,26–28] as well as flame-induced turbulence [29–31].

The previous discussion and review illustrate the popularity of spherically expanding premixed flames to study cellular instabilities. These instabilities, however, also manifest in burner-stabilized flames, for example, Bunsen flames. A typical laminar Bunsen flame is usually axisymmetric and constitutes a smooth cone-shaped flamefront. However, under certain conditions, a polyhedral structure may appear, where the otherwise smooth cone-shaped flame becomes wrinkled. Several straight ridges appear from the bottom and extend all the way to the tip of the conical flame and conform to a polyhedral geometry. Unlike the well-studied positively stretched expanding flame, the Bunsen flame has a dominant axial flow close to the nozzle [32], and the flame surface is negatively stretched. The cellular instabilities are promoted by negative stretch [33], and thus, they predominantly appear along radial lines in a Bunsen flame, which results in the structure of a polyhedral flame. Such polyhedral structure in a Bunsen flame was first observed by Smithells and Ingle [34] in rich benzene, pentane, and hexane mixture, which was subsequently confirmed to be caused due to a diffusive-thermal cellular instability.

Although relatively less-explored compared to its counterpart, the expanding flame, there have been a few foundational studies that paved the way for our current understanding of polyhedral Bunsen flames. For example, Guenoche and Markstein [35] reported that the transition between smooth and polyhedral flames can occur due to changes in flow rate, while Buckmaster [36] reported that the number of sides can vary greatly under various conditions. It was also shown that regions of polyhedral flames can have augmented or weakened burning, manifested by bright and dark edges, respectively, on flame chemiluminescence images [37,38]. It was also reported that the location of ridges in a polyhedral flame may not be stable, as evidenced by unidirectional, bi-directional, or chaotic rotation of the edges with rapid changes in fuel concentration [37]. The stability of polyhedral flames, in general, was shown to be strongly dependent on the amount of heat loss to the burner and hence influenced by burner (nozzle) geometry. Buckmaster [36] used linear stability analysis to determine several key parameters to identify the critical condition for the manifestation of polyhedral flames. Furthermore, the rotational instability of the polyhedral structures was analyzed by considering the interaction of two harmonic unstable modes. Subsequently, the rotation instability was further investigated by Gorman et al. [39].

While the above discussion highlights the detailed work that investigated polyhedral flames, there is a lack of systematic study to delineate the effects of various operating parameters on the stability and morphology of these flames. For example, in most studies, the experiments were conducted while changing two or more operating parameters, and hence, identification of their individual effects becomes challenging. Thus, we present a detailed experimental investigation of the dynamics and morphology of polyhedral flames and the effects of the adiabatic flame temperature (T_b), equivalence ratio (ϕ), and flow rate ($\dot{Q}$) on them. We conduct the study with practically relevant lean hydrogen and methane flames.

The rest of the manuscript is put forward in several sections. First, we discuss the experimental setup, diagnostic methods, and the mixture conditions studied. Subsequently, we present our primary findings and discuss the results in the context of flame theories. Finally, we conclude the manuscript with a summary of our investigation of polyhedral flames.

2. Experimental setup

Our experiments were conducted using a Bunsen burner designed with a cooling jacket to ensure constant temperature and prevent overheating of the burner tip. The detailed schematic of the experimental setup, along with the primary optical setup, is shown in Fig. 1. The central nozzle has an outer diameter of 15.2mm, while the inner diameter $D = 12.4$mm. We used a flat burner tip, which is made of brass. The geometry of the tip is critical since the flow field near the burner exit influences the flame configuration and stability.

The gaseous fuel (Hydrogen, H_2 or Methane, CH_4), Oxygen (O_2), and inert gases (Nitrogen, N_2 or Argon, Ar) were supplied in appropriate proportion from separate gas cylinders and were mixed in a small mixing chamber located upstream, before passing through the burner nozzle. The individual flow rates of these gases and the total volume flow rates were controlled by a number of digitally controlled mass flow controllers (Alicat MCR: ±0.2% full scale). Since we intend to study the dynamics of laminar flames, the total flow rate ($\dot{Q}$) was maintained to be smaller than 30SLPM, beyond which the flame loses its steady shape and shows turbulent-like behavior. Note that the transition to turbulent flame can be identified from high-speed side view images as the conical steady Bunsen flame geometry transforms into a highly unsteady wrinkled structure with a large brush thickness and short flame length. One can define a Reynolds number as $Re = \rho UD/\mu$, where ρ and μ are the density and dynamic viscosity of the premixed gas. The mean velocity (U) is related to the total volumetric flow rate by $U = 4\dot{Q}/(\pi D^2)$.

Most of the experiments were conducted using Hydrogen (H_2)-Oxygen (O_2)-Nitrogen (N_2) mixtures, which have practical importance in carbon-less combustion. We varied the H_2 to O_2 ratio or equivalence ratio (ϕ) to modulate Le, defined as the thermal to mass diffusivity of the mixture. For hydrogen flames, it is well-known that Le of the mixture decreases (or increases) with a decrease (or increase) in equivalence ratio (ϕ). The lean ($\phi < 1$) and rich ($\phi > 1$) hydrogen flames possess $Le < 1$ and $Le > 1$ mixtures, respectively [38]. Apart from H_2, a small set of experiments were conducted using Methane(CH_4)-Oxygen(O_2)-Argon(Ar) mixtures to confirm that the observed dynamics are fuel independent. Since the Le for $CH_4 - O_2 - N_2$ mixtures are close to unity, we used a heavier inert gas (Ar) to reduce the thermal diffusivity of the mixture and obtain the $Le < 1$ condition. Irrespective of the fuel, the adiabatic flame temperature T_b of the mixture was modulated by changing the ratio of oxygen and inert gas in the mixture. The fundamental flame properties, such as unstretched planar laminar flame speed, flame thickness, and adiabatic flame temperature, were evaluated through the PREMIXED module in Chemkin-Pro software, using GRI-3.0 [40] chemistry model. The conditions used in this study and their corresponding parameters are listed in Table 1.

In literature, there are several theoretical methods that can be used to obtain the mixture Lewis number [41]. Some of the common methods that have been proposed by various groups include Le based on deficient species [42], heat release-based weighted average [43], volume-based weighted average [44], the diffusivity of the fuel [45] etc. Here, we used the definition based on the global reaction scheme proposed by Addabbo et al. [46]. The effective Lewis number of the mixture is given by

$$Le = 1 + \frac{(Le_E - 1) + (Le_D - 1)\mathcal{A}}{1 + \mathcal{A}}, \tag{1}$$

where Le_D and Le_E are Lewis numbers of the deficient and excess species, respectively. $\mathcal{A} = 1 + Ze(\bar{\Phi} - 1)$ is the mixture strength. $Ze = E(T_b - T_0)/RT_b^2$ is the Zel'dovich number, R is the gas constant, T_b is the adiabatic flame temperature, T_0 is the unburned gas tem-

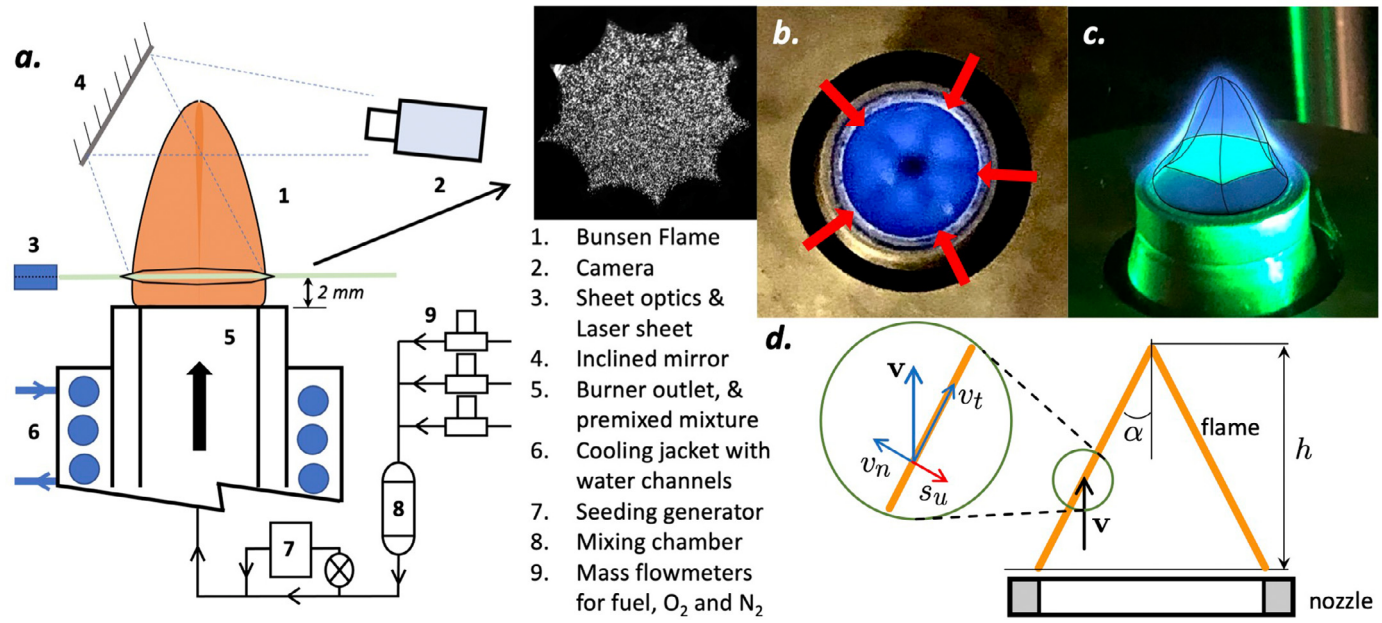

Fig. 1. **(a.)** Schematic of the experimental setup with primary components and flow controllers. (inset: a typical Mie scattering image of a polyhedral flame). **(b.)** The top view chemiluminescence of a polyhedral flame (lean $CH_4 - O_2 - Ar$ mixture). The flame is split into 5 cells, whose ridges are marked by arrows. **(c.)** Side view of the same flame displaying planar Mie-scattering of horizontal cross-section as illuminated by the laser sheet. **(d.)** Schematic showing the coordinate system for the laminar Bunsen flame.

Table 1
List of experimental conditions, where ϕ is the equivalence ratio and T_b is the adiabatic temperature, $s_{u,0}$ is the unstretched planar laminar flame speed.

Mixture	T_b(K)	ϕ	O_2%	*Le*	$s_{u,0}$(cm/s)
$H_2 - O_2 - N_2$	1300 ± 10	0.5	14.5	0.406	6.15
		0.6	12.1	0.432	6.31
		0.7	10.3	0.466	6.03
		0.85	8.5	0.562	6.04
$H_2 - O_2 - N_2$	1350 ± 10	0.5	15.4	0.412	9.11
		0.6	12.8	0.437	8.97
		0.7	11	0.474	9.02
		0.85	9	0.571	8.51
$H_2 - O_2 - N_2$	1400 ± 10	0.5	16.3	0.417	12.4
		0.6	13.6	0.443	12.38
		0.7	11.6	0.48	11.95
		0.85	9.5	0.579	11.42
$H_2 - O_2 - N_2$	1450 ± 10	0.5	17.2	0.421	16.3
		0.6	14.3	0.448	15.94
		0.7	12.3	0.487	15.96
		0.85	10	0.588	15.43
$H_2 - O_2 - N_2$	1500 ± 10	0.5	18.2	0.426	21.17
		0.6	15.1	0.454	20.43
		0.7	12.9	0.493	19.86
		0.85	10.6	0.598	20.17
$H_2 - O_2 - N_2$	1550 ± 10	0.5	19.2	0.431	26.56
		0.6	15.9	0.459	25.53
		0.7	13.6	0.5	24.91
$H_2 - O_2 - N_2$	1600 ± 10	0.5	20.2	0.436	32.52
$CH_4 - O_2 - Ar$	1888	0.5	22	0.954	22.77

perature, and E is the activation energy. We discuss how to evaluate the activation energy in the supplementary materials. $\bar{\Phi}$ is the mass ratio of excess, to the deficient species, with respect to the stoichiometric mixture and is equal to, and reciprocal of the equivalence ratio for the rich ($\bar{\Phi} = \phi$), and lean ($\bar{\Phi} = 1/\phi$) mixtures, respectively. Further details are provided in Addabbo et al. [46]. The calculated Lewis numbers for all the mixtures are listed in Table 1.

As expected, for all lean $H_2 - O_2 - N_2$ mixtures, *Le* is smaller than unity, and as the equivalence ratio increases, the *Le* increases.

As mentioned before, most of the experiments were performed with H_2, for which it was difficult to capture clear (blue) chemiluminescence images due to lack of CH^* in flames. As an alternative, we used planar Mie-scattering imaging to visualize the morphology of the Bunsen flames. For the Mie-scattering imaging, an Nd-YLF laser (wavelength 527nm) along with sheet-making optics was used to create an approximately 1mm thick laser sheet. The premixed gas mixture passing through the burner was seeded with D.E.H.S. (di-ethyl hexyl sebacate) droplets with a mean size of $1 - 2\mu$m, which scattered the laser light. The resultant Mie-scattering images were captured using a DSLR camera in our experiments. Near the flamefront, due to high temperature, these droplets evaporate, limiting the high seeding density only to the unburned side. Thus, when imaged, the Mie scattering from these seeding droplets displays the contour of the flamefront [31,47]. Since we are mostly interested in observing the polyhedral geometry, we visualized the cross-section of the flame by placing the laser sheet horizontally at a distance $\sim$2mm from the burner exit and imaging the illuminated zone from the top using a 45° mirror, as shown in Fig. 1. The inset of Fig. 1a shows a typical Mie-scattering image. For CH_4 flames, chemiluminescence images can also be captured to observe the global flame shape (Fig. 1b,c).

3. Results

To explore the morphology and transitional boundaries of polyhedral Bunsen flames, we first established the flame at a condition with fixed ϕ and T_b, by igniting the premixed gas emanating from the nozzle. Then, while keeping the mixture condition fixed, we increased or decreased the volumetric flow rate $\dot{Q}$ in small increments using the mass flow controllers. We waited for the flame to achieve a steady state after each incremental change and acquired images of the flame morphology at each condition. Here, it is important to note that a change in $\dot{Q}$ alters the length of a stable Bunsen flame. Furthermore, there exist two limits of $\dot{Q}$ between which a stable Bunsen flame can be established. When the

$\dot{Q}$ is smaller than a critical lower limit, the flame moves inside the burner tube, and flashback is observed. We used this flow condition as the lower critical point for each case. At a very high $\dot{Q}$, blow-off is observed, in that the flame detaches from the burner and extinguishes. There also exists a $\dot{Q}$ (approximately 30SLPM for the current burner) beyond which the flow emanating from the burner becomes turbulent. Recognizing that the presence of turbulence can significantly modify the transitional boundaries of cellular instabilities, in our experiments, we used this limit as the largest operational flow rate and limited our study to $\dot{Q} \leq$ 30SLPM. The general shape and strength of the flame are also sensitive to change in ϕ or *Le*. This is a common behavior of stretched flames and has been extensively discussed in the literature in the context of smooth, stable laminar flames. Following the above-mentioned procedure, we performed experiments at fixed ϕ (or *Le*) and T_b for cases detailed in Table 1, and identified the range of flow rates for which polyhedral flames can be observed. Simultaneously, we also monitored the changes in the morphology of the polyhedral structures by analyzing the Mie-scattering images.

3.1. Regime maps

By repeated experiments for a large range of ϕ (or *Le*) and T_b, we identified the range of $\dot{Q}$ over which polyhedral instabilities were observed. The observations can be presented in the form of regime maps, which we will discuss next.

3.1.1. T_b dependence

To delineate the effect of T_b on the polyhedral cellular instability, we plotted regime maps at fixed ϕ (or *Le*) for lean $H_2 - O_2 - N_2$ flames. These maps were constructed by identifying the state of the flame over a range of $\dot{Q}$ for various T_bs. The regime maps for four different ϕ (or *Le*) are shown in Fig. 2. Different symbols were used in the regime map to identify the state of the flames, e.g. stars: polyhedral flame, circles: smooth laminar flame, square: flashback. We notice that at any T_b, the lowest flow rate required for polyhedral flame ($\dot{Q}_{min}$) was limited by flashback (green circles). This observation is, in general, true for all the conditions we have studied. The regime map also shows that, with increase in T_b, the $\dot{Q}_{min}$ increases (Fig. 2a–d). This can be attributed to the increased flame speed ($S_{u,0}$) with T_b and hence, a larger critical flow speed (or $\dot{Q}$) required to avoid flashback.

At a fixed T_b, for $\dot{Q} > \dot{Q}_{min}$, we observe the continued existence of the polyhedral structure over a range of flow rate until we reach another critical value $\dot{Q}_{max}$. At this critical flow rate $\dot{Q}_{max}$, the flame becomes smooth and devoid of any polyhedral structures (Fig. 2a–d). This transition from polyhedral to a smooth morphology due to an increase in flow rate was also reported in previous studies [36,37,48]. However, no clear explanation was provided about the underlying physics of this transition. Later in the manuscript (Section 3.3), we will show that this transition can be explained by an analysis of residence time.

In Fig. 2, we can also observe that the $\dot{Q}_{max}$ decreases as we move to higher T_b. The flow rate regime over which polyhedral flames can be observed, thus, can be defined as $\dot{Q}_{min} < \dot{Q} < \dot{Q}_{max}$. Since both the $\dot{Q}_{min}$ and $\dot{Q}_{max}$ increase with T_b, there exists a critical value ($T_{b,m}$) for a fixed ϕ (or *Le*), beyond which polyhedral flames can not be observed. This critical temperature, $T_{b,m}$ increases as the ϕ (and *Le* for H_2-flames *Le*) decreases ($T_{b,m} = 1600$K for $\phi = 0.5$ and $T_{b,m} = 1500$K for $\phi = 0.85$). Comparison of the regime maps for four different ϕ (or *Le*) (Fig. 2a–d) confirms that, as we decrease *Le*, the range of conditions favorable for a polyhedral flame becomes larger. This extension is caused by the stronger diffusional-thermal instability for smaller *Le* flames.

3.1.2. Le dependence

Next, we will discuss the role of *Le* on the instability by potting the state of the flames as a function of ϕ and $\dot{Q}$ at fixed T_b. Fig. 3 shows such regime maps for four different T_bs. It is to be noted that for lean ($\phi < 1$) $H_2 - O_2 - N_2$ flames, *Le* is less than unity, and it decreases with a decrease in ϕ [38]. In general, we observe a similar trend between all ϕ (or *Le* conditions) in that, at any given ϕ, the polyhedral flames are observed between an upper and lower limit of flow rates $\dot{Q}_{min} < \dot{Q} < \dot{Q}_{max}$. The $\dot{Q}_{min}$, which is bounded by flashback, decreases with an increase in ϕ or *Le*. This is consistent with the literature on flashback [49,50], which has shown that the critical flow rate required for flashback decreases with an increase in *Le*.

At the other extreme, $\dot{Q}_{max}$, at which the polyhedral flame transforms into a smooth flame, also decreases with an increase in ϕ or *Le* (Fig. 3). Furthermore, the overall range of flow rate for which the polyhedral flames are observed becomes larger with a decrease in T_b (Fig. 3a–d). We will show that the boundary depends on the residence time scale in Section 3.3.

3.2. Morphology analysis

In this section, we will discuss the changes in the morphology of the polyhedral flames with changes in the operating conditions. Previous experimental studies have shown that the mixture condition and flow rate can alter the number of ridges of a polyhedral flame. However, a detailed description and a systematic investigation are lacking. In general, at the onset of instability, the otherwise smooth conical Bunsen flame forms ridges along the length of the flame, which presents as a polyhedral structure. At this stage, the horizontal cross-section of the flame appears to be a polygon as shown in Fig. 1c. As we vary the $\dot{Q}$ or *Le*, we observe changes in the number of ridges or the number of sides of the polygon, as seen in the horizontal cross-section. Within our experimental conditions, for lean H_2 flames, the number of the ridges (N) varied from 7 to 20, while for the CH_4 flame, the variation in N was much narrower, from 3 to 7.

Figure 4 shows the typical horizontal cross-sections of polyhedral flames. The top row consists of images from lean $H_2 - O_2 - N_2$ flames at five different ϕ or *Le* at fixed $\dot{Q} \approx 10$ SLPM and $T_b =$ 1300K. We notice that from left to right (a1 to a5), the *Le* of the mixture increases, and the number of ridges of the polyhedral structure, N, decreases. In the second row of Fig. 4, the cross sections of CH_4 flames are shown. These images correspond to flames at different flow rates but at fixed *Le* ($\phi = 0.5$) and $T_b \approx 1888$K. In particular, from left to right (b1 to b4), $\dot{Q}$ is decreasing, which also reduces the number of ridges (N) in the polyhedral geometry.

To explain these observed dynamics and to analyze the flame morphologies, a dispersion relation will be used. While different forms of dispersion relations for flamefront instability have been developed by various research groups, including Pelce and Clavin [51], Matalon and Matkowsky [52,53] and Frankel and Sivashinsky [54], we will use the dispersion relation derived by Buckmaster [36]. However, other dispersion relations will qualitatively depict similar dynamics. Buckmaster [36] expressed the dispersion relation as

$$\tilde{\omega} = -4\tilde{k}^4 - \tilde{k}^2\left(1 + \frac{lJ_s}{2\tilde{T}_b^2}\right) - \frac{\theta(\tilde{T}_s - \tilde{T}_b + J_s)}{2\tilde{T}_b^2}. \quad (2)$$

Note that all the variables in this expression are in non-dimensional forms, as shown in [55]. $\tilde{\omega}$ is the non-dimensional growth rate, $\tilde{k}$ is the non-dimensional wavenumber. J_s is the mass flux fraction of the mixture through the burner, expressed as

$$J_s = \frac{\tilde{T}_b^2}{\theta}\sqrt{2\ Da\ Le\ \exp(-\frac{\theta}{\tilde{T}_b})}. \quad (3)$$

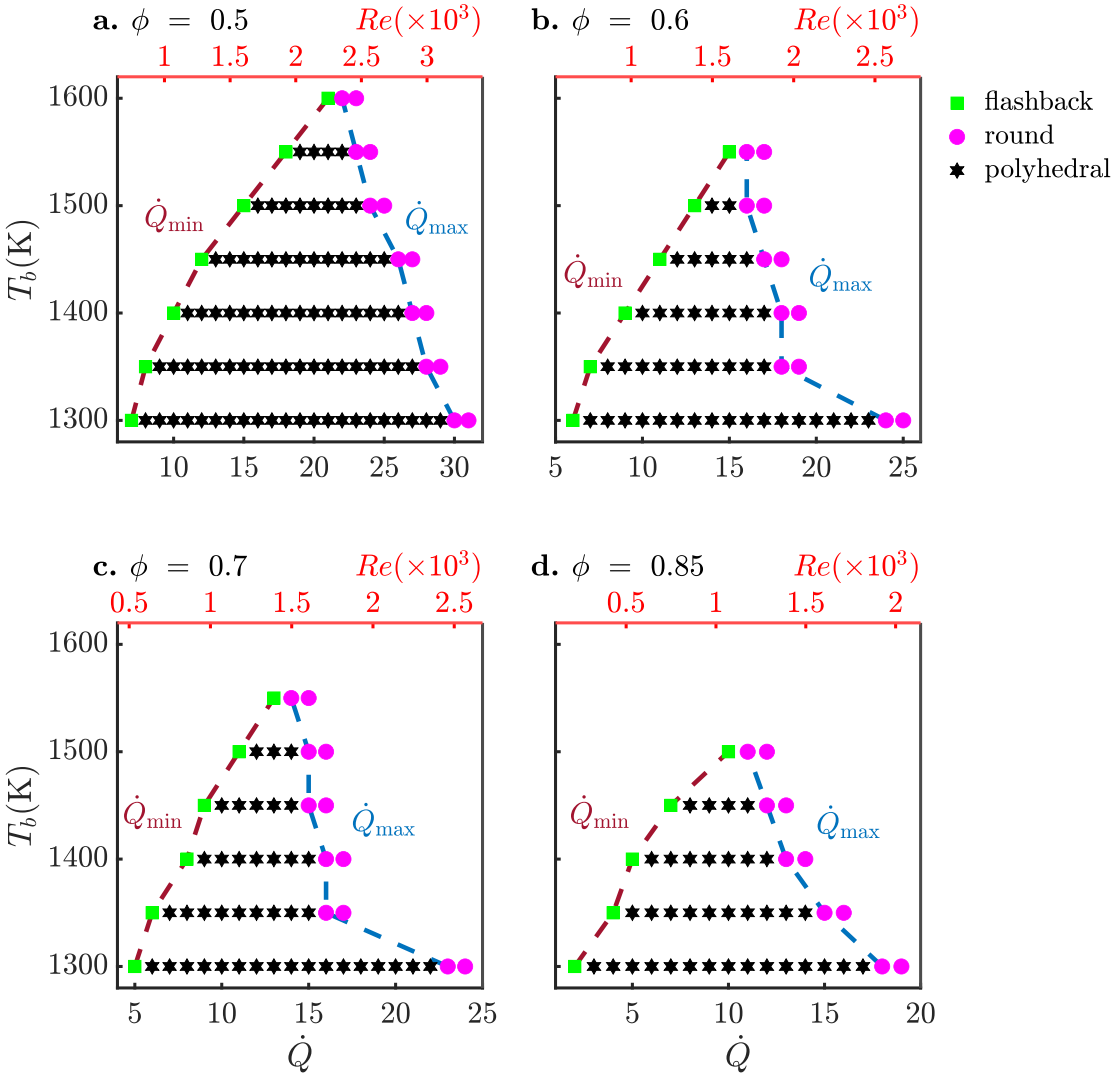

Fig. 2. Regime map for $H_2 - O_2 - N_2$ flames at fixed *Le* or ϕ. Flame states are shown as a function of $\dot{Q}$ *Re* and flame temperature (T_b). (**a**) $\phi = 0.5$, (**b**) $\phi = 0.6$, (**c**) $\phi = 0.7$, (**d**) $\phi = 0.85$. As T_b increases, the range of flow rate that polyhedral flames appear evidently reduces, and ultimately, no polyhedral structure can be observed above a certain T_b for the given ϕ.

Here, $\tilde{T}_s$ is the non-dimensional temperature of the burner surface, $\tilde{T}_b$ is the non-dimensional adiabatic flame temperature, θ is the non-dimensional activation energy (a brief description of how the activation energy is evaluated can be found in the supplementary material). The temperatures, in the dispersion relation, are non-dimensionalized by a temperature scale defined as $T_c = T_b - T_0$, where T_0 is the unburned gas temperature. *Da* is the Damkohler number and $l = \theta(1 - Le^{-1})$ is a measure of *Le*. Eq. (2) provides a range of wavenumber for which the growth rate is positive, and hence, the instability can manifest, and polyhedral structures are observed. The $\tilde{k}$ values where $\tilde{\omega} = 0$ draw the boundary of stability as shown in Fig. 5. The figure shows the typical range of wavenumbers, for which the flames are unstable as a function of *Le* (Fig. 5a).

The second term on the right-hand side of Eq. (2) demonstrates the Lewis number effect through the quantity, *l*. For $Le < 1$ (> 1), the *l* is negative (positive) which augments (suppresses) $\tilde{\omega}$, and hence the instability. This is evidenced in Fig. 5a in the form of a critical $Le(\approx 1)$, beyond which the flame is stable for all $\tilde{k}$.

The number of ridges, *N*, however, is dictated by the critical (dimensional) wavenumber k_c corresponding to the maximum growth rate. This can be assessed by setting $\partial\tilde{\omega}/\partial\tilde{k} = 0$ in Eq. (2), which leads to the non-dimensional critical wavenumber, $\tilde{k}_c = \sqrt{(-1/8)(1 + lJ_S/(2T_b^2))}$. By using the definition of non-dimensional wavenumber $\tilde{k}_c = k_c L_c$ [55], where $L_c = \mathcal{D}_{\text{th}}/U$ is the characteristic length scale, and $\mathcal{D}_{\text{th}}$ is the thermal diffusivity, we can express

$$k_c = \frac{4\dot{Q}}{\pi D^2 \mathcal{D}_{\text{th}}} \sqrt{-\frac{1}{8}\left(1 + \frac{lJ_S}{2T_b^2}\right)}. \tag{4}$$

Since $N \sim Dk_c$, and *D* (the burner diameter) is a constant, we can expect the number of ridges to be proportional to the critical wavenumber ($N \sim k_c$). To assess the role of *Le* on the number of ridges, we plotted the k_c as a function of the *Le* for fixed $\tilde{T}_b$ in Fig. 5a (red line). The plot shows that k_c decreases with an increase in *Le*, hence we observe a reduction in the number of edges (*N*) in Fig. 4a as ϕ (or *Le*) is increased for a lean H_2 flame. Eq. (4) also shows that for a fixed *Le* and T_b, the k_c (and *N*) decreases as the flow rate $\dot{Q}$ decreases, as shown in Fig. 5b, which corroborates with the experimental observation for CH_4 flames (Fig. 4b).

3.3. Scaling of $\dot{Q}_{max}$

While discussing the regime maps in Section 3.1, we identified that there exists an upper limit of flow rate ($\dot{Q}_{max}$), beyond which

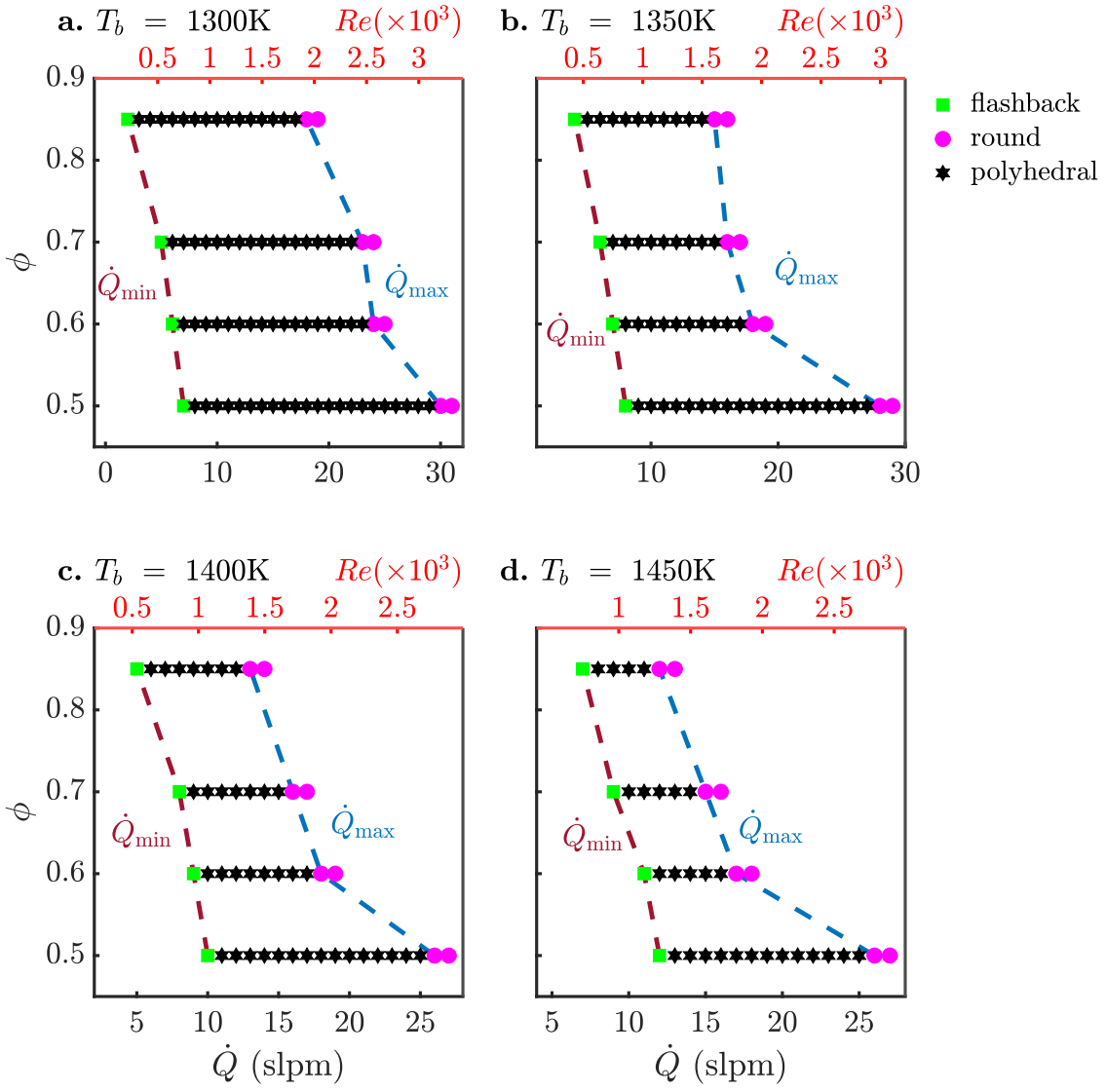

Fig. 3. Regime map for $H_2 - O_2 - N_2$ flames at fixed T_b. Flame states are shown as functions of $\dot{Q}$ *Re* and ϕ. (**a**) T_b = 1300K, (**b**) T_b = 1350K, (**c**) T_b = 1400K, (**d**) T_b = 1450K.

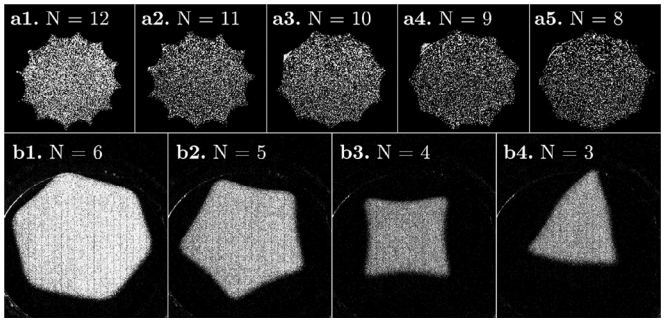

Fig. 4. A few samples of Mie-scattering images of a horizontal cross-section of polyhedral flames, the numbers of edges *N* are noted in the images. The first row (from **a1** to **a5**) corresponds to a lean $H_2 - O_2 - N_2$ flame with T_b = 1300K, $\dot{Q}$ = 10SLPM. **a1.** ϕ = 0.4, 12 ridges; **a2.** ϕ = 0.5, 11 ridges; **a3.** ϕ = 0.6, 10 ridges; **a4.** ϕ = 0.7, 9 ridges; **a5.** ϕ = 0.85, 8 ridges. As ϕ increases, the number of edges decreases. The second row (from **b1** to **b4**) corresponds to lean $CH_4 - O_2 - Ar$ flame with ϕ = 0.5, oxygen ratio at 22%, from left to right: $\dot{Q}$ reduces from 5 to 2SLPM. As $\dot{Q}$ decreases, the number of edges decreases.

polyhedral instability disappears. This observation was reported in previous studies [36], although no quantitative reasoning was provided. In this study, we also notice that, with an increase in *Le* or T_b, $\dot{Q}_{max}$ decreases. In the following, we will derive a scaling relation for this $\dot{Q}_{max}$ and discuss its dependence on the operating conditions. Physically, the polyhedral instability requires a finite time (τ_g) to develop, which is inversely proportional to the maximum growth rate ($\tau_g \sim 1/\omega_c$). Here, ω_c corresponds to the maximum growth rate, which can be derived from the dispersion relation in Eq. (2). On the other hand, the flow emanating from the nozzle has a residence time scale (τ_r). We expect that for the instability to develop, the residence time must be larger than the growth time for the instability ($\tau_r > \tau_g$). A similar argument for slot burners was also made by Rosen and Axelbaum [56] to derive the limiting condition for instabilities. In the present study, we can define the τ_r as the time taken by a fluid particle to reach the flame height *h* from the nozzle exit and can be expressed as

$$\tau_r \sim \frac{h/\cos\alpha}{v_t} = \frac{h}{U\cos^2\alpha} = \frac{\pi D^2 h}{4\dot{Q}\cos^2\alpha}. \quad (5)$$

Here, the tangential component of the flow velocity along the flame surface is $v_t = U/\cos\alpha$, where α is the half cone angle of the Bunsen flame (shown in Fig. 1d). By assuming the Bunsen flame to be a perfect cone and using the theoretical relation between unstretched planar flame speed ($s_{u,0}$) and half cone angle

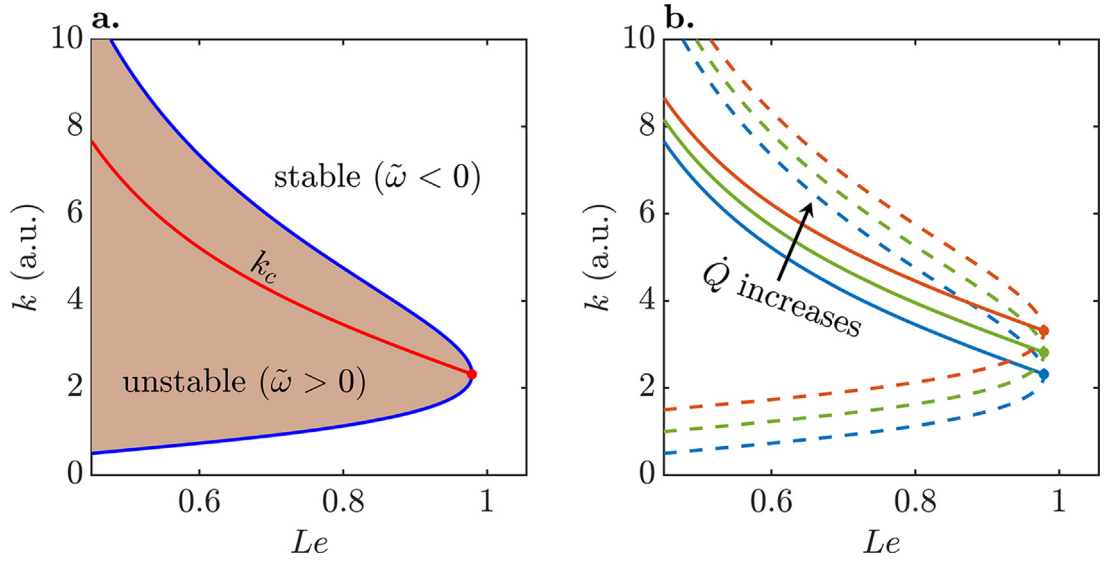

Fig. 5. (a.) Stability map as function of *Le* indicating the unstable modes of polyhedral flames. The shaded area corresponds to conditions with a positive growth rate and denotes the presence of cellular instability and polyhedral flames. The red line indicates critical wavenumber, $\tilde{k}_c$, corresponding to the maximum growth rate, which determines the number of edges in polyhedral flames. **(b.)** Stability map as $\dot{Q}$ changes.

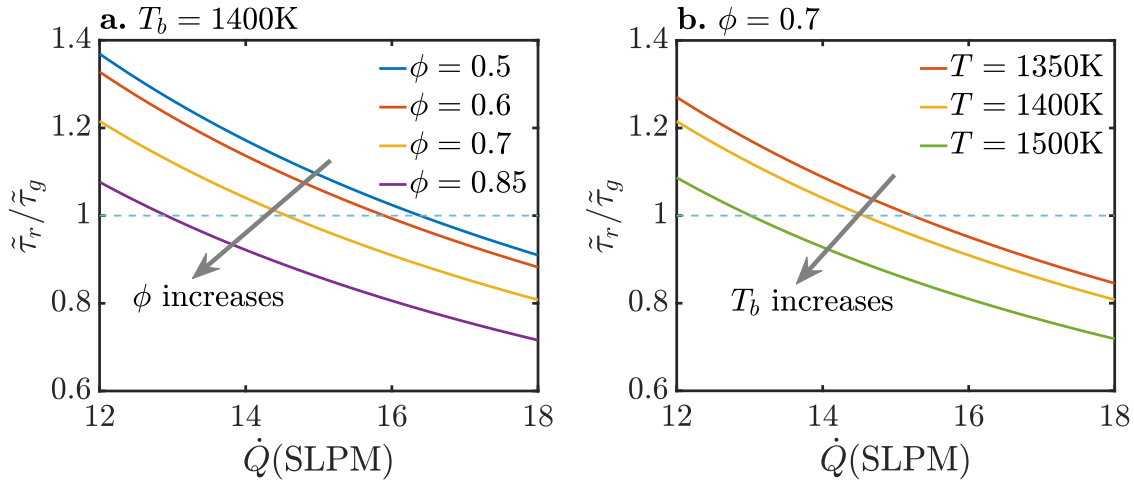

Fig. 6. $\tilde{\tau}_r/\tilde{\tau}_g$ as function of $\dot{Q}$ for (a) different ϕ and (b) T_b based on the scaling analyzes. $\dot{Q}$ corresponding to $\tilde{\tau}_r/\tilde{\tau}_g = 1$, refers to the theoretical estimation of $\dot{Q}_{max}$.

$(\cos\alpha = \sqrt{1-(s_{u,0}/U)^2})$ [38], we can rewrite the τ_r as

$$\tau_r \sim \frac{\pi D^2 h}{4\dot{Q}\left[1-\left((\pi/4)s_{u,0}D^2/\dot{Q}\right)^2\right]} \tag{6}$$

Both Eqs. (5) and (6) show that the residence time, τ_r decreases with increase in flow rate ($\dot{Q}$), for a fixed mixture condition (ϕ and T_b). When the $\dot{Q}$ becomes so large that $\tau_r < \tau_g$, the cellular structure cannot develop due to limited residence time. Thus, there exists a maximum flow rate, $\dot{Q}_{max}$, beyond which polyhedral structure cannot be observed. This upper limit, $\dot{Q}_{max}$, can be theoretically estimated with the limiting condition of $\tau_r/\tau_g \approx 1$. By substituting the expression for the critical wavenumber $\tilde{k}_c$ (Eq. (4)), in the dispersion relation (Eq. (2)), we find the non-dimensional timescale for instability

$$\tilde{\tau}_g = \tilde{\omega}_c^{-1} = \left[\frac{1}{16}\left(1+\frac{lJ_s}{2\tilde{T}_b^2}\right)^2 - \frac{\theta(\tilde{T}_s-\tilde{T}_b+J_s)}{2\tilde{T}_b^2}\right]^{-1}. \tag{7}$$

On the other hand, we can evaluate the non-dimensional residence time ($\tilde{\tau}_r = \tau_r/t_F$) by using Eq. (6). Here, $t_F = \delta_0/s_{u,0}$ is the flame timescale. In Fig. 6(a) we plotted $\tilde{\tau}_r/\tilde{\tau}_g$ for a fixed T_b and few different ϕ or *Le*. First, we observe that for any given ϕ, $\tilde{\tau}_r/\tilde{\tau}_g$ decreases with increase in $\dot{Q}$, and crosses the theoretical limit of $\tilde{\tau}_r/\tilde{\tau}_g = 1$ at a critical $\dot{Q}$. This value identifies the theoretical estimation of $\dot{Q}_{max}$, beyond which instability cannot be observed. Furthermore, we observe that the $\tilde{\tau}_r/\tilde{\tau}_g$ lines shift to left as ϕ increases, and hence, the theoretical $\dot{Q}_{max}$ becomes smaller with increase in ϕ or *Le*. This corroborates with the experimental findings in Fig. 2. Similarly, in Fig. 6(b) we plotted $\tilde{\tau}_r/\tilde{\tau}_g$ for a fixed ϕ and a few different T_bs. We observe that, as T_b increases, the theoretical limit of the higher flow rate $\dot{Q}_{max}$ decreases, a trend also observed in experiments (Fig. 3). We also notice that the theoretical $\dot{Q}_{max}$ values are in the same range of experimentally observed values. Some discrepancies are expected as the scaling analysis involves several simplifications in assessing the timescales.

4. Conclusion

In summary, we have presented a comprehensive experimental study of polyhedral Bunsen flames. Hydrogen was used as the primary fuel for the experimental investigation. Hydrogen is consid-

ered to be one of the viable alternate fuels to limit the emission of greenhouse gases from combustors. Although preferred for reducing emissions, owing to its sub-unity *Le*, lean hydrogen-air mixtures are prone to cellular instabilities, such as polyhedral Bunsen flames.

We studied the dynamics and morphology of such flames for a range of equivalence ratios (or *Le*), T_b, and $\dot{Q}$. We discerned that the polyhedral structures of Bunsen flame can occur for $Le < 1$ conditions only for a certain range of flow rates. The lower bound of the flow rate is limited by flashback, which increases with T_b, but decreases with *Le*. The upper bound of the flow rate at which a polyhedral flame transforms into a smooth flame is controlled by the residence time scale τ_r. For a Bunsen flame, this upper limit decreases with both T_b and *Le*. This behavior can be attributed to the competition between the growth rate of instabilities and the residence time of the flow. A scaling analysis was performed to derive a theoretical estimation for this upper bound of the flow rate for which polyhedral instability can be observed. Regime maps constructed using the experimental data for a large range of conditions demonstrate that for a fixed *Le*, the range of flow rate for which polyhedral flames are observed decreases with an increase in T_b. Furthermore, there exists a maximum temperature beyond which polyhedral Bunsen flames are not observed for any flow rate.

Subsequently, we have also carefully identified the number of edges or ridges in the polyhedral structure formed during the instability. Experimentally, we found that the number of ridges decreases with an increase in *Le* at a fixed flow rate and flame temperature. On the other hand, the number of edges increases with an increase in flow rate for a fixed *Le* and flame temperature. These behaviors were systematically observed for both hydrogen and methane flames. A detailed analysis of the dispersion relation and the critical wavenumber for maximum growth rate was performed. The critical wavenumber corresponding to the maximum growth rate of the instability, which controls the number of edges, was shown to decrease and increase with an increase in the mixture *Le* and the $\dot{Q}$, respectively.

Data availability statement

The data can be made available upon reasonable request.

Declaration of Competing Interest

The authors declare that they have no known competing financial interests or personal relationships that could have appeared to influence the work reported in this paper.

Acknowledgments

This work was supported by US National Science Foundation (CBET-Grant number: 2053671).

Supplementary material

Supplementary material associated with this article can be found, in the online version, at doi:10.1016/j.combustflame.2022.112585

References

[1] J.O. Abe, A. Popoola, E. Ajenifuja, O.M. Popoola, Hydrogen energy, economy and storage: review and recommendation, Int. J. Hydro. Energy 44 (29) (2019) 15072–15086.
[2] H.J. Plass Jr, F. Barbir, H.P. Miller, T.N. Veziroğlu, Economics of hydrogen as a fuel for surface transportation, Int. J. Hydrog. Energy 15 (9) (1990) 663–668.
[3] G.A. Karim, Hydrogen as a spark ignition engine fuel, Int. J. Hydrog. Energy 28 (5) (2003) 569–577.
[4] L.M. Das, Hydrogen-oxygen reaction mechanism and its implication to hydrogen engine combustion, Int. J. Hydrog. Energy 21 (8) (1996) 703–715.
[5] D. Cecere, E. Giacomazzi, A. Ingenito, A review on hydrogen industrial aerospace applications, Int. J. Hydrog. Energy 39 (20) (2014) 10731–10747.
[6] P. Clavin, Dynamic behavior of premixed flame fronts in laminar and turbulent flows, Prog. Energy Combust. 11 (1) (1985) 1–59.
[7] G.I. Sivashinsky, On the intrinsic dynamics of premixed flames, Philos. Trans. R. Soc. A 332 (1624) (1990) 135–148.
[8] G. Darrieus, Propagation dun front de flamme, La Technique Moderne 30 (1938) 18.
[9] L.D. Landau, On the theory of slow combustion, Acta Physicochim. URSS 19 (1) (1944) 77–85.
[10] G.I. Sivashinsky, Diffusional-thermal theory of cellular flames, Combust. Sci. Technol. 15 (3–4) (1977) 137–145.
[11] G.I. Sivashinsky, Instabilities, pattern formation, and turbulence in flames, Ann. Rev. Fluid Mech. 15 (1) (1983) 179–199.
[12] G.I. Sivashinsky, Some developments in premixed combustion modeling, Proc. Combust. Inst. 29 (2) (2002) 1737–1761.
[13] S. Chaudhuri, V. Akkerman, C.K. Law, Spectral formulation of turbulent flame speed with consideration of hydrodynamic instability, Phys. Rev. E 84 (2) (2011) 026322.
[14] G. Troiani, F. Creta, M. Matalon, Experimental investigation of darrieus–landau instability effects on turbulent premixed flames, Proc. Combust. Inst. 35 (2) (2015) 1451–1459.
[15] S. Yang, A. Saha, Z. Liu, C.K. Law, Role of Darrieus–Landau instability in propagation of expanding turbulent flames, J. Fluid. Mech. 850 (2018) 784–802.
[16] Z. Liu, V.R. Unni, S. Chaudhuri, C.K. Law, A. Saha, Local statistics of laminar expanding flames subjected to Darrieus Landau instability, Proc. Combust. Inst. (2020), doi:10.1016/j.proci.2020.06.118.
[17] C.K. Law, G. Jomaas, J.K. Bechtold, Cellular instabilities of expanding hydrogen/propane spherical flames at elevated pressures: theory and experiment, Proc. Combust. Inst. 30 (2005) 159–167.
[18] M.Z. Haq, Correlations for the onset of instabilities of spherical laminar premixed flames, J. Heat Transf. 127 (12) (2005) 1410–1415.
[19] Z.-Y. Sun, F.-S. Liu, X.-C. Bao, X.-H. Liu, Research on cellular instabilities in outwardly propagating spherical hydrogen-air flames, Int. J. Hydrog. Energy 37 (9) (2012) 7889–7899, doi:10.1016/j.ijhydene.2012.02.011.
[20] C. Clanet, G. Searby, First experimental study of the Darrieus-Landau instability, Phys. Rev. Lett. 80 (17) (1998) 3867.
[21] J.F. Yu, R. Yu, X.Q. Fan, M. Christensen, A.A. Konnov, X.-S. Bai, Onset of cellular flame instability in adiabatic CH4/o2/CO2 and CH4/air laminar premixed flames stabilized on a flat-flame burner, Combust. Flame 160 (7) (2013) 1276–1286.
[22] D. Bradley, Instabilities and flame speeds in large-scale premixed gaseous explosions, Philos. Trans. R. Soc. A 357 (1764) (1999) 3567–3581.
[23] F. Wu, G. Jomaas, C.K. Law, An experimental investigation on self-acceleration of cellular spherical flames, Proc. Combust. Inst. 34 (1) (2013) 937–945.
[24] S. Yang, A. Saha, F. Wu, C.K. Law, Morphology and self-acceleration of expanding laminar flames with flame-front cellular instabilities, Combust. Flame 171 (2016) 112–118.
[25] J. Beeckmann, R. Hesse, S. Kruse, A. Berens, N. Peters, H. Pitsch, M. Matalon, Propagation speed and stability of spherically expanding hydrogen/air flames: experimental study and asymptotics, Proc. Combust. Inst. 36 (1) (2017) 1531–1538.
[26] C.R. Bauwens, J.M. Bergthorson, S.B. Dorofeev, Experimental study of spherical-flame acceleration mechanisms in large-scale propane–air flames, Proc. Combust. Inst. 35 (2) (2015) 2059–2066.
[27] Y.A. Gostintsev, A.G. Istratov, Y.V. Shulenin, Self-similar propagation of a free turbulent flame in mixed gas mixtures, Combust. Explos. Shock Waves 24 (5) (1988) 563–569.
[28] Y. Xie, J. Wang, X. Cai, Z. Huang, Self-acceleration of cellular flames and laminar flame speed of syngas/air mixtures at elevated pressures, Int. J. Hydrog. Energy 41 (40) (2016) 18250–18258.
[29] N. Fogla, F. Creta, M. Matalon, Effect of folds and pockets on the topology and propagation of premixed turbulent flames, Combust. Flame 162 (7) (2015) 2758–2777.
[30] R. Lamioni, P.E. Lapenna, G. Troiani, F. Creta, Flame induced flow features in the presence of darrieus-Landau instability, Flow Turbul. Combust. 101 (4) (2018) 1137–1155.
[31] Z. Liu, V.R. Unni, S. Chaudhuri, R. Sui, C.K. Law, A. Saha, Self-turbulization in cellularly unstable laminar flames, J. Fluid Mech. 917 (2021).
[32] S. Ishizuka, K. Miyasaka, C.K. Law, Effects of heat loss, preferential diffusion, and flame stretch on flame-front instability and extinction of propane/air mixtures, Combust. Flame 45 (1982) 293–308.
[33] G.I. Sivashinsky, C.K. Law, G. Joulin, On stability of premixed flames in stagnation-point flow, Combust. Sci. Technol. 28 (3–4) (1982) 155–159.
[34] A. Smithells, Xvi.note on the structure of luminous flames, J. Chem. Soc. Trans. 61 (1892) 217–226.
[35] H. Guenoche, G.H. Markstein, Nonsteady Flame Propagation, Pergamon Press, New York, 1964, p. 107.
[36] J. Buckmaster, Polyhedral flamesan exercise in bimodal bifurcation analysis, SIAM J. Appl. Math. 44 (1) (1984) 40–55.
[37] S.H. Sohrab, C.K. Law, Influence of burner rim aerodynamics on polyhedral flames and flame stabilization, Combust. Flame 62 (3) (1985) 243–254.
[38] C.K. Law, Combustion Physics, Cambridge University Press, 2010.

[39] M. Gorman, C.F. Hamill, M. El-Hadi, K.A. Robbins, Rotating and modulated rotating states of cellular flames, Combust. Sci. Technol. 98 (1–3) (1994) 25–35.
[40] G.P. Smith, D.M. Golden, M. Frenklach, N.W. Moriarty, B. Eiteneer, M. Goldenberg, C.T. Bowman, R.K. Hanson, S. Song, W.C. Gardiner, et al., GRI 3.0, 1999, (http://www.me.berkeley.edu/gri_mech/).
[41] N. Bouvet, F. Halter, C. Chauveau, Y. Yoon, On the effective lewis number formulations for lean hydrogen/hydrocarbon/air mixtures, Int. J. Hydrog. Energy 38 (14) (2013) 5949–5960.
[42] W.K. Lewis, The evaporation of a liquid into a gas, Trans. ASME. 44 (1922) 325–340.
[43] C.K. Law, G. Jomaas, J.K. Bechtold, Cellular instabilities of expanding hydrogen/propane spherical flames at elevated pressures: theory and experiment, Proc. Combust. Inst. 30 (1) (2005) 159–167.
[44] S. Muppala, M. Nakahara, N.K. Aluri, H. Kido, J.X. Wen, M.V. Papalexandris, Experimental and analytical investigation of the turbulent burning velocity of two-component fuel mixtures of hydrogen, methane and propane, Int. J. Hydrog. Energy 34 (22) (2009) 9258–9265.
[45] F. Dinkelacker, B. Manickam, S. Muppala, Modelling and simulation of lean premixed turbulent methane/hydrogen/air flames with an effective lewis number approach, Combust. Flame 158 (9) (2011) 1742–1749.
[46] R. Addabbo, J.K. Bechtold, M. Matalon, Wrinkling of spherically expanding flames, Proc. Combust. Inst. 29 (2) (2002) 1527–1535.
[47] S. Chaudhuri, A. Saha, C.K. Law, On flame–turbulence interaction in constant–pressure expanding flames, Proc. Combust. Inst. 35 (2) (2015) 1331–1339.
[48] S. Gutman, R.L. Axelbaum, G.I. Sivashinsky, On bunsen burner polyhedral flames, Combust. Sci. Technol. 98 (1–3) (1994) 57–70.
[49] V.N. Kurdyumov, E. Fernandez, A. Linan, Flame flashback and propagation of premixed flames near a wall, Proc. Combust. Inst. 28 (2) (2000) 1883–1889.
[50] V. Kurdyumov, E. Fernandez-Tarrazo, J.-M. Truffaut, J. Quinard, A. Wangher, G. Searby, Experimental and numerical study of premixed flame flashback, Proc. Combust. Inst. 31 (1) (2007) 1275–1282.
[51] P. Pelce, P. Clavin, Influence of hydrodynamics and diffusion upon the stability limits of laminar premixed flames, J. Fluid Mech. 124 (1982) 219–237.
[52] M. Matalon, B.J. Matkowsky, Flames as gasdynamic discontinuities, J. Fluid Mech. 124 (1982) 239–259.
[53] M. Matalon, B.J. Matkowsky, On the stability of plane and curved flames, SIAM J. Appl. Math. 44 (2) (1984) 327–343.
[54] M.L. Frankel, G.I. Sivashinsky, The effect of viscosity on hydrodynamic stability of a plane flame front, Combust. Sci. Technol. 29 (3–6) (1982) 207–224.
[55] J.D. Buckmaster, G.S.S. Ludford, Theory of Laminar Flames, Cambridge Monographs on Mechanics, Cambridge University Press, 1982, doi:10.1017/CBO9780511569531.
[56] L.J. Rosen, R.L. Axelbaum, Suppression of cellular structure in slot-burner flames, Combust. Flame 126 (1–2) (2001) 1433–1444.